PCCP

Unusual liquid–liquid phase transition in aqueous mixtures of a well-known dendrimer†

Viviana C. P. da Costa and Onofrio Annunziata*

Liquid–liquid phase separation (LLPS) has been extensively investigated for polymer and protein solutions due to its importance in mixture thermodynamics, separation science and self-assembly processes. However, to date, no experimental studies have been reported on LLPS of dendrimer solutions. Here, it is shown that LLPS of aqueous solutions containing a hydroxyl-functionalized poly(amido amine) dendrimer of fourth generation is induced in the presence of sodium sulfate. Both the LLPS temperature and salt–dendrimer partitioning between the two coexisting phases at constant temperature were measured. Interestingly, our experiments show that LLPS switches from being induced by cooling to being induced by heating as the salt concentration increases. The two coexisting phases also show opposite temperature response. Thus, this phase transition exhibits a simultaneous lower and upper critical solution temperature-type behavior. Dynamic light-scattering and dye-binding experiments indicate that no appreciable conformational change occurs as the salt concentration increases. To explain the observed phase behavior, a thermodynamic model based on two parameters was developed. The first parameter, which describes dendrimer–dendrimer interaction energy, was determined by isothermal titration calorimetry. The second parameter describes the salt salting-out strength. By varying the salting-out parameter, it is shown that the model achieves agreement not only with the location of the experimental binodal at 25 °C but also with the slope of this curve around the critical point. The proposed model also predicts that the unusual temperature behavior of this phase transition can be described as the net result of two thermodynamic factors with opposite temperature responses: salt thermodynamic non-ideality and salting-out strength.

1. Introduction

Liquid–liquid phase separation (LLPS) of aqueous solutions containing biological and synthetic macromolecules has received much attention from a theoretical and practical point of view.[1–5] This phenomenon has been used not only to characterize molecular interactions in solution[6–8] but also to represent an important process for applications in the fields of materials science,[9–12] separation science,[13,14] catalysis,[15,16] biology[2–4,17,18] and biotechnology.[5,19,20]

Dendrimers are hyperbranched macromolecules that consist of a multifunctional central core to which branching units are sequentially added, resulting in a tree-like structure.[21] The number of branching points, when going radially from the core towards the surface, defines the dendrimer generation (G). Dendrimers can be synthesized in a wide range of generations. Furthermore, the terminal groups on the dendrimer outer shell

can be readily modified into a high number and a variety of functional groups in order to tune both the solubility of these macromolecules in a given solvent and their binding affinity towards target ligands.[21,22]

The dendrimer tree-like structure gives rise to the formation of internal cavities. This structural property is very important for host–guest interactions[23–25] and the applications of dendrimers as drug-delivery carriers,[26–28] nanoreactors,[25,29,30] extracting agents[31,32] and as building blocks or templates for self-assembly processes.[33–36]

There is a substantial overlap between the scopes of dendrimers and LLPS applications. For example, the LLPS of dendrimer solutions could be used to reversibly produce a dendrimer-rich phase (coacervates[9]) and a remaining liquid phase significantly depleted in dendrimer concentration. In the case of catalysis, a thermoregulated formation of coacervates of dendrimer nanoreactors could be employed to separate these catalytic materials from the reaction products. In the case of extraction, coacervation could be used to separate the molecules sequestered by the host dendrimers from solution with applications to purification and drug loading. Finally, the combination of LLPS and chemical crosslinking could be applied to produce dendrimer

Department of Chemistry, Texas Christian University, Fort Worth, Texas 76129, USA. E-mail: O.Annunziata@tcu.edu; Fax: +1 817 257-5851; Tel: +1817 257-6215

† Electronic supplementary information (ESI) available: Experimental data and the thermodynamic model. See DOI: 10.1039/c5cp04642d

28818 | *Phys. Chem. Chem. Phys.*, 2015, **17**, 28818–28829

This journal is © the Owner Societies 2015

nanoparticles and microspheres with high guest loading capacity, relevant to drug delivery applications.

In relation to phase separation, there are a few studies on thermoresponsive dendrimers showing temperature-induced dendrimer aggregation in aqueous solutions.[37–43] The aggregation is induced by *ad hoc* modifications of the dendrimer structure by either incorporating well-known thermoresponsive groups,[37,38] or by an appropriate balance of hydrophilic and hydrophobic moieties.[43] In relation to LLPS, there are theoretical studies on dendrimer systems.[44–46] However, to our knowledge, there is no experimental study on this phase transition.

Here, we report an experimental and theoretical investigation on the LLPS of aqueous solutions of a poly(amido amine) (PAMAM) dendrimer.[21] There are many experimental investigations on PAMAM dendrimers relevant to drug delivery,[47,48] catalysis[25,29,49] and synthesis of metal nanoclusters.[50] Furthermore, there is also a broad range of related fundamental studies on dendrimer conformation and flexibility.[51–66]

The dendrimer chosen in this work is the hydroxyl-functionalized PAMAM of fourth generation (PAMAM–OH, G4). This dendrimer is expected to be preferentially hydrated in aqueous solutions due to the hydrophilic nature of the hydroxyl terminal groups. Thus, LLPS may be observed in the presence of salting-out agents as described for proteins[7] and polymers.[14,67] In this work, we show that LLPS can be induced in the presence of sodium sulfate. The observed phase transition has a unique thermal behavior, which is qualitatively different from that normally reported in the case of other macromolecules.

2. Experimental section

2.1 Materials

Hydroxyl-functionalized poly(amido amine) dendrimers of fourth generation (PAMAM–OH, G4) were purchased from Dendritech, Inc (Midland) in a methanol solution. Methanol was removed by drying dendrimer samples in a vacuum oven at 50 °C. The dried samples were then dissolved in water and the drying procedure was repeated to remove residual amounts of methanol. Deionized water was passed through a four-stage Millipore filter system to provide high-purity water for all the experiments. Dendrimer–water stock solutions (20–40% w/w) with a total mass of ≈ 0.5 g were then prepared by weight. The dendrimer molecular weight used to calculate molar concentrations was 14.3 kg mol^{-1}. Sodium sulfate was purchased from J.T. Baker (New Jersey, USA). A salt–water stock solution of 1 L was prepared and its composition (18.31% w/w) was determined from density measurements on properly diluted solutions using a digital density meter (Mettler/Paar, DMA40), thermostated at 25.00 ± 0.01 °C. Density values were converted into the corresponding concentrations using the known[68] relationship between density and salt composition. The concentration of this stock solution was periodically checked. Copper sulfate and *N,N*-dimethylindoaniline dye (phenol blue) and *N*-(2-acetamido)-2-aminoethanesulfonic acid (ACES) were purchased from Sigma Aldrich (Missouri, USA). Triethanolamine

and silicone oil were purchased from Fisher Scientific (New Hampshire, USA).

2.2 Turbidity assay

The LLPS temperature, T_{ph}, was determined by measuring the turbidity of ternary dendrimer–salt–water samples as a function of temperature. A ternary homogenous small sample (≈ 100 μL) with a given composition was prepared by mixing known amounts of water, dendrimer and salt stock solutions. The known weight fractions of dendrimer and salt in the ternary mixture were then converted into dendrimer volume fraction, ϕ_D, and salt molar concentration, C_S, after estimating the sample density using the known[68] volumetric properties of binary sodium sulfate–water solutions and the dendrimer specific volume specific volume of 0.817 g cm^{-3}.[69] More details are available in the ESI.† All samples for turbidity measurements were allowed to equilibrate for two days at a temperature at which they were homogeneous. We note that T_{ph} was found to strongly depend on salt concentration. Thus, errors in T_{ph} values due to water evaporation were minimized by layering silicon oil on our small samples.

The turbidity meter is comprised of a programmable circulating bath (1197P, VWR), a calibrated thermocouple (±0.1 °C), and a homemade optical cell, in which the initially transparent sample (optical path of 0.4 cm) and a thermocouple probe are located. Collimated light from a solid state laser (633 nm, 5 mW, Coherent) passes through the sample and its transmittance is recorded using a photodiode detector coupled with a computer-interfaced optical meter (1835-C Newport).[70] After recording the transmitted intensity of the transparent sample, the temperature of the bath is changed at a constant rate of ±0.5 °C min^{-1}. We identify T_{ph} as the temperature at which a sharp decrease in intensity is observed (cloud point). Values of $T_{ph}(C_S,\phi_D)$ are reported in the ESI.†

2.3 Salt–dendrimer partitioning

Samples for partitioning measurements must be prepared at dendrimer concentrations of $\approx 25\%$ (w/w) in order to produce biphasic systems with roughly equal amounts of dendrimer-rich and dendrimer-poor phases. Due to the high dendrimer concentration and material availability, the size of samples was ≈ 0.5 mL. To circumvent challenges related to the small sample size and viscosity, the characterization of dendrimer–salt partitioning required the development of a new experimental procedure to first equilibrate and then separate the two coexisting liquid phases. This procedure can also be extended to LLPS studies of other macromolecules such as proteins. Furthermore, as described below, we have developed two assays to determine the dendrimer and salt concentration in the two phases. Samples for partitioning measurements were prepared as follows. A known amount of dendrimer and salt stock solutions, and water were mixed together so that the final system consisted of two coexisting liquid phases at room temperature. Capped test tubes containing our samples were then mixed vigorously using a vortex stirrer for 5 min at room temperature to facilitate equilibration. These samples were then immersed in a temperature-controlled

water bath at 25.0 °C. It is important to note that sample shaking did not lead to appreciable sample mixing due to the sample small volume (500 μL) and viscosity. Thus, sample mixing was achieved by test-tube rotation (0.2 rpm for two days) leading to cyclic sample inversions inside the water bath. Afterwards, samples were positioned vertically and held stationary to allow for macroscopic phase separation of the two coexisting liquid phases by gravity. When a clear interface between the two phases is observed, aliquots (100–200 μL) from the bottom phase (I) and the top phase (II) were transferred into small test tubes and weighted. The aliquot from the bottom solution taken after the intermediate region containing the liquid–liquid interface was removed by suction using a needle connected to a vacuum pump. The two separated samples taken from the bottom and top phases were both centrifuged (Allegra™ 25R centrifuge, Beckman Coulter) to verify their homogeneity. The composition of the two phases was then characterized using a spectrophotometric assay (for dendrimer) and a potentiometric assay (for salt). The composition of the two coexisting phases was reported as dendrimer volume fraction and salt molar concentration, $(\phi_D^{(I)}, C_S^{(I)})$ and $(\phi_D^{(II)}, C_S^{(II)})$, respectively.

2.4 Spectrophotometric assay

Our assay is based on previous binding studies on copper–dendrimer systems.[50] These studies show that the absorbance of copper ions at 610 nm is negligible and significantly increases with dendrimer concentration. Thus, a calibration curve was prepared by measuring copper absorbance at 610 nm (DU 800 spectrophotometer, Beckman Coulter) as a function of dendrimer concentration. A small aliquot of bottom or top phase was first diluted. An excess of copper sulfate was then added to ensure that all dendrimer binding sites were occupied. Sodium sulfate was found to have no effect on sample absorbance within our experimental salt concentration range.

2.5 Potentiometric assay

Salt concentration was determined by utilizing a sodium ion-selective electrode (Accumet). A small aliquot of a given sample was first properly diluted with water. A known excess (90%) of an ionic strength adjustor (triethanolamine–water solution, 5.3% v/v, pH 9.5) was then added to the diluted sample. A calibration curve was prepared by measuring the electrode electrical potential as a function of sodium sulfate concentration (reported as $\ln C_S$). The effect of dendrimer concentration was also characterized. All potentiometric measurements were performed under moderate sample stirring at room temperature. Our calibration procedure was repeated every time the composition of a new set of samples needed to be characterized.

2.6 Dye binding assay

Our binding assay was based on measuring the absorbance of phenol blue at 646.5 nm (DU 800 spectrophotometer, Beckman Coulter). A stock solution of phenol blue in water (0.02 mM) was prepared by extensively stirring dye–water suspensions at room temperature under dark conditions. The obtained stock solution was then filtered (Nalgene filter, 0.2 μm pore size).

Solutions were then prepared by mixing the phenol blue stock solution with water, dendrimer and sodium sulfate stock solutions. For all solutions, the dye concentration was kept constant at 0.01 M. The dendrimer concentration was also kept constant at 1.73 mM. This concentration was chosen by verifying that the absorbance of 0.01 M dye solutions at 646.5 nm significantly decreases as dendrimer concentration increases up to about 1.7 mM. Thus, the fraction of dye bound to the dendrimer is close to maximum under these conditions. The sodium sulfate concentration in our solutions was increased up to 0.7 M. Solutions with higher salt concentrations could not be prepared due to solubility limitations of phenol blue and sodium sulfate in their corresponding aqueous stock solutions. All absorbance measurements were promptly performed on the freshly prepared solutions and then repeated after 24 hours to allow for binding to occur and reach equilibrium. Control experiments on dendrimer-free dye solutions were also performed. All samples were stored under dark conditions during the incubation time of 24 hours.

2.7 Isothermal titration calorimetry

The excess internal energy associated with dendrimer–dendrimer interactions was measured by Isothermal Titration Calorimetry (ITC) using the MicroCal iTC200 System from GE Healthcare Life Sciences.[71] All experiments were performed at 25.0 °C. In these experiments, dendrimer aqueous salt solution were exhaustively dialyzed against an aqueous salt buffer (ACES, pH 7.0, 0.10 M; sodium sulfate, 0.030 M; ionic strength, 0.14 M) and concentrated by ultrafiltration. The final dendrimer concentration was determined using the spectrophotometric assay described in Section 2.4. Dendrimer volume fractions ranged from $\phi_D^0 = 0.10$ to $\phi_D^0 = 0.19$. Small aliquots of these solutions ($\nu = 2.0$ μL) were sequentially injected (19 injections, titrant) using a rotating syringe into the vigorously stirred sample cell (syringe rotation, 1000 rpm) containing the aqueous salt buffer (titrand). The ITC cell volume is $V = 203.4$ μL. To minimize the effects related to minor differences in the thermodynamic activities of the buffer components, ionic strength and pH, the filtrate obtained from the ultrafiltration procedure was used as the titrand. The dendrimer volume fraction inside the ITC cell after injection k was calculated using[71]

$$\phi_D^{(k)} = k\nu\phi_D^0/(V + 0.5k\nu) \qquad (1)$$

where the volumetric factor, $V + 0.5k\nu$, takes into account concentration reductions due to the small sample displacement outside the ITC cell. Each injection produced an exothermic peak on a plot showing the power required to maintain the sample and reference cells at the same temperature as a function of time. The differential heat associated with each injection is calculated as the area of the corresponding measured peak and normalized with respect to the number of moles of the titrant. Specifically, the differential heat per mole of the titrant is given by

$$q^{(k)} = [(V + 0.5\nu)(V_D Q^{(k)}/V) - (V - 0.5\nu)(V_D Q^{(k-1)}/V)]/(\nu\phi_D^0) + k_{ITC}\phi_D^{(k)} \qquad (2)$$

28820 | *Phys. Chem. Chem. Phys.*, 2015, **17**, 28818–28829

This journal is © the Owner Societies 2015

where $Q^{(k)}$ is the cumulative heat after injection k, $Q^{(0)} = 0$, $V_D = 11.7$ dm^3 mol^{-1} is the dendrimer molar volume and k_{ITC} is a parameter characterizing a small baseline correction. Setting $k_{ITC} = 0$ gives an error lower than 5% in the determined energy parameters. The use of the factors, $V \pm 0.5 \ k\nu$, instead of V represents small corrections taking into account sample displacement outside the ITC cell.[71] The mathematical expression shown for $V_D Q^{(k)}/V$ in Section 3 is then inserted into eqn (2). Note that superscript "k" will be omitted in Section 3 since $V_D Q/V$ is a continuum function of the sample composition. The method of least squares was then applied to the differential heat data according to eqn (2). Values of $q^{(k)}(\phi_D, \phi_D^0)$ are reported in the ESI.†

2.7 Dynamic light scattering

Diffusion measurements by dynamic light scattering (DLS) were performed at 25.0 ± 0.1 °C and 37.0 ± 0.1 °C on dendrimer–salt–water solutions. All samples were filtered through a 0.02 μm filter (Anotop 10, Whatman). The experiments were carried out on a light scattering apparatus built using the following main components: He–Ne laser (35 mW, 632.8 nm, Coherent Radiation), a manual goniometer and a thermostat (Photocor Instruments), a multi-tau correlator, an APD detector and software (PD4042, Precision Detectors).[72] All experiments were performed at the scattering angle of $\theta = 90°$. The scattering vector $q = (4\pi n/\lambda)\sin(\theta/2)$ was calculated using $n = 1.33$ and $\lambda = 632.8$ nm. The scattered-intensity correlation functions were analyzed using a regularization algorithm (Precision Deconvolve 32, Precision Detectors).[73] All experimental correlation functions correspond to monomodal diffusion-coefficient distributions. The DLS diffusion coefficient, D_{DLS}, was taken as the z-average diffusion coefficient of the obtained distributions. Values of $D_{DLS}(\phi_D, C_S, T)$ are reported in the ESI.†

3. Results and discussion

We explored the effect of salts on the phase behavior of aqueous solutions of PAMAM–OH, G4 aqueous solutions. While no phase separation was observed in the presence of a mild salting-out agent such as sodium chloride, we found that LLPS can be induced in the presence of sodium sulfate, a stronger salting-out agent according to the Hofmeister series.[8] LLPS occurred at ionic strengths of the order of one or higher. At these high ionic strengths, the salting-out action of salt ions on the somewhat positively charged[74] dendrimer macro ions is not expected to be related to electrostatic interactions[75] but rather to dendrimer preferential hydration.[76–80]

In the following sections, our experimental results on the LLPS of this dendrimer–salt–water system and other related experiments are reported. A theoretical thermodynamic model is then developed to describe our experimental findings.

3.1 Effect of salt concentration on LLPS temperature

The composition of the ternary dendrimer–salt–water system is given by the dendrimer volume fraction, ϕ_D, and salt molar concentration, C_S. The LLPS boundary is described by the LLPS

temperature, T_{ph}, as a function of C_S and ϕ_D. We have experimentally characterized T_{ph} as a function of C_S at several values of ϕ_D. Interestingly, these experiments revealed a peculiar temperature behavior. Specifically, LLPS switches from being induced by lowering temperature to being induced by increasing temperature as salt concentration increases and dendrimer concentration correspondingly decreases. Our results are shown in Fig. 1A–D. Representative temperature–turbidity profiles showing LLPS induced by cooling or heating are shown in Fig. 1A and C, respectively. In Fig. 1B and D, we report our phase-boundary results obtained at relatively low (B, 0.3–0.5 mol dm^{-3}) and high (D, 0.7–1.4 mol dm^{-3}) salt concentrations. In all cases, T_{ph} was found to strongly depend on salt concentration. Both the positive slopes of the T_{ph} curves in Fig. 1B and the corresponding negative slopes in Fig. 1D are consistent with sodium sulfate promoting LLPS. Interestingly, experiments in a narrow range of intermediate salt concentrations revealed that the turbidity of initially homogenous samples was found to increase by both cooling and heating as shown in Fig. 2.

3.2 Salt–dendrimer partitioning

At a fixed temperature, LLPS yields the formation of two coexisting liquid phases with compositions $(C_S^{(I)}, \phi_D^{(I)})$ and $(C_S^{(II)}, \phi_D^{(II)})$ for phases I and II, respectively. We have experimentally characterized these compositions at 25 °C. Our results are reported in Table 1 together with the corresponding partitioning coefficients defined as $\Delta C_S/\Delta \phi_D \equiv (C_S^{(II)} - C_S^{(I)})/(\phi_D^{(II)} - \phi_D^{(I)})$. The negative values of $\Delta C_S/\Delta \phi_D$ reflect the salting-out mechanism; *i.e.*, the preferential hydration[80] of both solute components leads to salt-rich (I) and dendrimer-rich (II) coexisting phases. Note that the reported $\phi_D^{(II)}$ values of 0.3 and higher correspond to the short average particle–particle distance of about 4 nm, consistent with the formation of dendrimer coacervates. Turbidity experiments revealed that the separated coexisting phases display opposite temperature responses, consistent with our results reported in Section 3.1. Thus, this phase transition exhibits a simultaneous lower and upper critical solution temperature-type behavior.

Our values in Table 1 can be used to estimate the critical dendrimer volume fraction, $\phi_D^{(c)}$. This was obtained by the linear extrapolation of $(\phi_D^{(I)} + \phi_D^{(II)})/2$ to $|\phi_D^{(II)} - \phi_D^{(I)}|^{1/\beta} \to 0$, with $\beta = 0.325$ (Ising exponent) and $\beta = 0.5$ (mean-field exponent).[17] From the corresponding plots, we found that $\phi_D^{(c)}$ is between 0.15 and 0.18, which correspond to salt critical concentrations, $C_S^{(c)}$, ranging from 0.6 to 0.7 mol dm^{-3}. Similarly, we have also used the $\Delta C_S/\Delta \phi_D$ values to extract the limiting partition coefficient at the critical point, $(\partial C_S/\partial \phi_D)_T$. Since these ratios show an error of $\approx 20\%$, the corresponding extrapolation error is also large. We found that $(\partial C_S/\partial \phi_D)_T$ is between -3 and -2 mol dm^{-3}. Details are reported in the ESI.†

3.3 Dendrimer diffusion coefficient

The peculiar temperature behavior of this phase transition may be caused by salt-induced conformational changes in the flexible dendrimers. To examine this hypothesis, we determined the dendrimer hydrodynamic radius, R_h, at both low and high salt
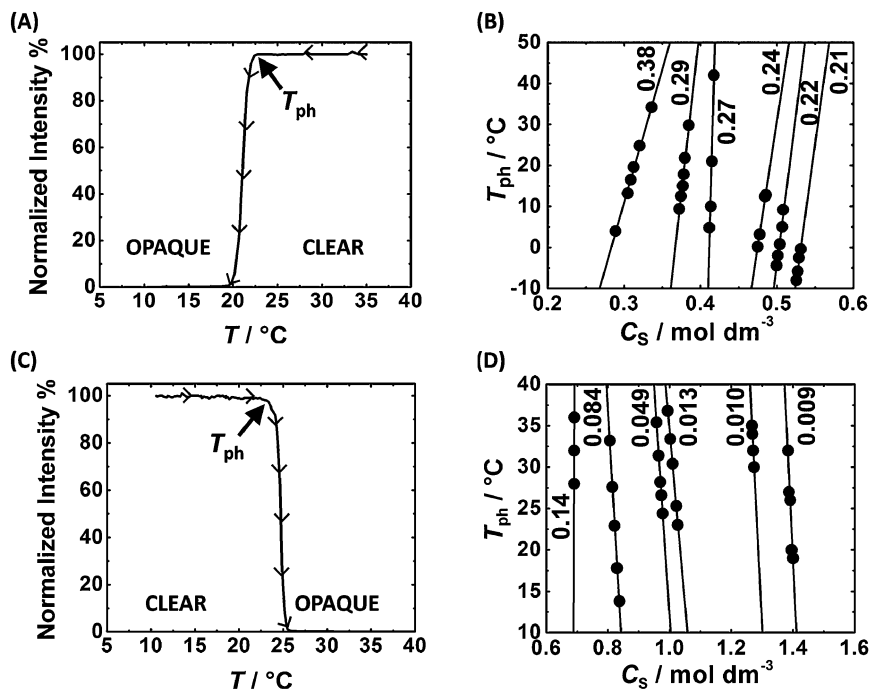
This journal is © the Owner Societies 2015

Phys. Chem. Chem. Phys., 2015, **17**, 28818–28829 | **28821**

Fig. 1 (A) Normalized-transmitted-intensity profile corresponding to LLPS induced by decreasing temperature, T. The LLPS temperature, T_{ph}, was identified as the temperature at which a sharp decrease in intensity is observed. (B) The corresponding T_{ph} values increase as salt concentration, C_S, increases. The numbers associated with each curve identify the corresponding value of constant dendrimer volume fractions. The solid lines are linear fits to the experimental data. (C) Normalized-transmitted-intensity profile corresponding to LLPS induced by increasing temperature. (D) The corresponding T_{ph} values decrease as salt concentration increases.
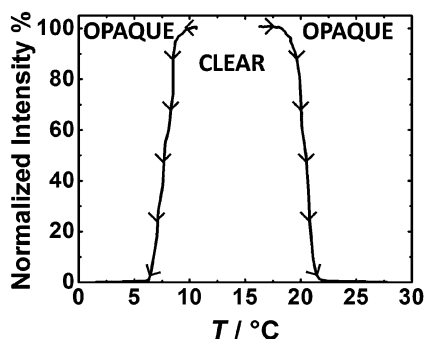

Fig. 2 Normalized-transmitted-intensity profile observed for the dendrimer–salt–water system at $C_S = 0.51$ mol dm^{-3} and $\phi_D = 0.20$.

Table 1 Salt–dendrimer partitioning parameters at 25 °C

$C_S^{(I)}$/mol dm^{-3}	$\phi_D^{(I)}$	$C_S^{(II)}$/mol dm^{-3}	$\phi_D^{(II)}$	$(\Delta C_S/\Delta \phi_D)$/mol dm^{-3}	q
1.01	0.030	0.36	0.36	−2.0	0.25
1.19	0.038	0.33	0.35	−2.8	0.34
1.47	0.031	0.31	0.40	−3.1	0.32
1.66	0.003	0.18	0.52	−2.9	0.26

concentrations by measuring the DLS dendrimer diffusion coefficient, D_{DLS}, as a function of ϕ_D. At $\phi_D = 0$, D_{DLS} becomes the dendrimer tracer-diffusion coefficient, D_0, and the Stokes–Einstein equation,[81] $R_h = k_B T/(6\pi\eta D_0)$, can be applied, with η being the known[82] viscosity of the salt–water system and k_B the Boltzmann constant. According to the Stokes–Einstein equation,

it is convenient to calculate the normalized diffusion coefficient, $(6\pi\eta/k_B T)D_{DLS}$, since it represents the inverse of an apparent hydrodynamic radius. In Fig. 3, we plot this coefficient as a function of ϕ_D at low (0.05 mol dm^{-3}) and high (1 mol dm^{-3}) salt concentrations and two temperatures, 25 and 37 °C. Experimental data were examined according to $D_{DLS} = D_0(1 + k_D \phi_D)$, and the values D_0 and k_D, obtained by applying the method of least squares, are reported in Table 2 together with the corresponding values of R_h. In all cases, the hydrodynamic
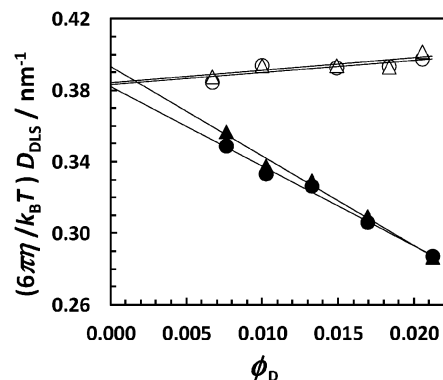

Fig. 3 Normalized DLS diffusion coefficient as a function of dendrimer volume fraction, ϕ_D, at two salt concentrations, $C_S = 0.044$ mol dm^{-3} (open circles, 25 °C; open triangles, 37 °C) and 0.51 mol dm^{-3} $C_S = 0.949$ mol dm^{-3} (closed circles, 25 °C; closed triangles, 37 °C). The solid lines are linear fits through the data.

Table 2 DLS parameters

C_S/mol dm^{-3}	T/°C	D_0/10^{-9} m^2 s^{-1}	η/10^{-3} kg m^{-1} s^{-1}	R_h/nm	k_D
0.044	25.0	0.0920 ± 0.0010	0.909	2.61 ± 0.03	1.8 ± 0.4
0.949	25.0	0.0615 ± 0.0006	1.357	2.62 ± 0.03	−11.6 ± 0.4
0.044	37.0	0.1236 ± 0.0014	0.706	2.60 ± 0.03	1.8 ± 0.4
0.949	37.0	0.0852 ± 0.0009	1.048	2.54 ± 0.03	−12.7 ± 0.4

radius was found to be 2.6 nm within the experimental error. Thus, salt and temperature have no appreciable effect on the dendrimer size.

We now turn our attention to the values of k_D in Table 2. Since these are positive at low salt concentration, dendrimer–dendrimer interactions are repulsive under these conditions.[83,84] On the other hand, k_D becomes negative at high salt concentration. This indicates that dendrimer–dendrimer interactions become more attractive as salt concentration increases, consistent with the salting-out mechanism. In Table 2, we can also see that the effect of temperature on k_D is small.

3.4 Dendrimer–dye binding

Dendrimer conformational changes need not cause large changes in the dendrimer size. Thus, we also characterized the effect of salt concentration on the binding affinity of the dendrimer to phenol blue, a dye that possesses an absorption band with a maximum at 646.5 nm in water.[85] As the polarity of the dye environment decreases, its absorbance at 646.5 nm correspondingly decreases. Thus, the binding of the dye to dendrimers will reduce the absorbance at 646.5 nm due to its less polar properties. Since dendrimer cavity accessibility and surface properties are expected to change in the presence of conformational changes, we expect that the dye spectrophotometric properties be sensitive to these changes. Our results in Fig. 4 show that dendrimer–dye binding occurs. However, no appreciable change in absorbance is observed as salt concentration increases. Thus, our experimental results are consistent with salt having no appreciable effect on the dendrimer conformational state.
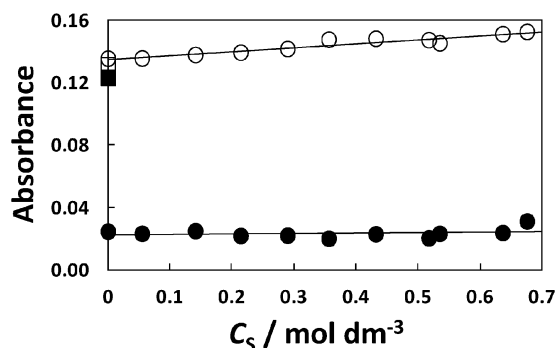

Fig. 4 Absorbance of phenol blue as a function of salt concentration, C_S, measured for freshly prepared solutions (open circles) and after 24 hours (solid circles) at room temperature at ϕ_D = 0.020 (solid circles, dye-to-dendrimer molar ratio, ≈6 × 10^{-3}). The solid lines are linear fits through the data. The open and the solid squares at C_S = 0, represent the absorbance of the dendrimer-free solution measured for a freshly prepared solution and after 24 hours, respectively.

3.5 Thermodynamic model

In this section, we develop a thermodynamic model that can be used to describe the phase behavior of dendrimer aqueous solutions. Our goal is to identify an equation of state for the dendrimer particles, which can then be used to compute the LLPS boundary. Here, we assume that dendrimers adopt a compact conformational state consistent with the presence of a strong salting-out agent. Since dendrimers are globular particles, the hard-sphere suspension[86] is an appropriate reference system for the proposed model. This reference system has been normally used for other globular macromolecules such as proteins.[87] To the equation of state of hard spheres, we add an energetic contribution describing dendrimer–dendrimer interactions. This contribution will be supported by our ITC experiments (see Section 3.6). Finally, to describe dendrimer–salt interactions, we consider the theory of preferential hydration and the two-domain model developed by Timasheff[76] and Record[77] in relation to protein–salt interactions in water.

According to the two-domain model, the preferential hydration of globular macromolecules in the presence of salting-out salts can be described by considering the existence of two domains.[77–79] The first domain is represented by the salt–water layers around the dendrimer macromolecule. This local domain is in chemical equilibrium with a bulk domain, representing the salt–water remaining solution. Since dendrimers interact with the salt and water molecules in their vicinity, the concentration of salt in the local domain is different from that of the unperturbed bulk domain. If dendrimer preferential hydration occurs, the salt concentration in the local domain is lower than that of the bulk domain. This corresponds to salting-out conditions. Thus, the local domain consists of the dendrimer particles and their adjacent salt-depleted aqueous layer. For strong salting-out agents such as sodium sulfate, the salt concentration in the local domain can be thought to be negligible.

The existence of the salt-depleted layer increases the chemical potential of a macromolecule by an amount that is equal to the reversible work performed against salt osmotic pressure in order to maintain salt ions outside the local domain. The presence of salt-depleted layers favors LLPS and other macromolecular condensation processes because the contacts between macromolecules reduce the overall volume of the local domain, thereby reducing the work contribution to the macromolecule chemical potential. Note that this description is analogous to that used to describe the condensation of colloidal particles in the presence of non-adsorbing polymers.[88,89]

According to the two-domain model, the thermodynamic properties of the salt in the bulk domain are the same as those of a binary salt–water large reservoir in equilibrium dialysis with the ternary mixture through a membrane not permeable to the dendrimer particles. The pressure difference between the ternary mixture and the binary reservoir is the osmotic pressure of the dendrimer particles. It can then be shown that (see ESI† for details)

$$p = p_D - (1 - \alpha + \alpha'\phi_D)p_s \qquad (3)$$

where $p \equiv \Pi V_D/RT$, $p_D \equiv \Pi_D V_D/RT$, and $p_s \equiv \Pi_S V_D/RT$ are unitless reduced pressure parameters, with Π being the osmotic

This journal is © the Owner Societies 2015

Phys. Chem. Chem. Phys., 2015, **17**, 28818–28829 | **28823**

pressure of the dendrimer particles, Π_D being the corresponding contribution in the absence of bulk domain, Π_S being the salt osmotic pressure of the binary reservoir (and the bulk domain) in the ternary mixture, $V_D = 11.7 \text{ dm}^3 \text{ mol}^{-1}$ is the dendrimer molar volume, R the ideal-gas constant and T the absolute temperature. The quantity α in eqn (3) is the volume fraction of the bulk domain in the ternary mixture, with $\alpha' \equiv d\alpha/d\phi_D$. If the salt molar concentration in the binary reservoir is C_S^*, the salt concentration in the ternary mixture is $C_S = C_S^* \cdot \alpha(\phi_D)$.

The salt osmotic pressure contribution, p_S, can be related to the known[90] temperature-dependent osmotic coefficient $\varphi(C_S^*, T)$ using

$$p_S = \gamma_D \nu_S \varphi(C_S^*, T) C_S^* / C_W^* \tag{4}$$

where $\gamma_D \equiv V_D/V_W = 645$, $\nu_S = 3$ for sodium sulfate, and C_W^* is the water molar concentration in the binary reservoir. At a given C_S^*/C_W^*, the salt osmotic coefficient is known to increase with temperature for sodium sulfate (see ESI†).

For a suspension of identical hard spheres with volume fraction, ϕ_D, the bulk-domain volume fraction, $\alpha(\phi_D, T)$, can be described as the probability of a successful insertion of a distinct test hard sphere with radius equal to the thickness of the salt-depleted layer (local domain). This implies that $\alpha(\phi_D, T)$ can be obtained from the excess chemical potential of the test particle, $(-RT \ln \alpha)$. We choose the expression of α obtained from the Mansoori–Carnahan–Starling–Leland equation of state for a binary hard-sphere mixture:[91,92]

$$\alpha = (1 - \phi_D)\exp[-A\eta_D - B\eta_D^2 - C\eta_D^3 + D\ln(1 + \eta_D)] \tag{5}$$

where $\eta_D \equiv \phi_D/(1 - \phi_D)$, $A \equiv 3q + 6q^2 - q^3$, $B \equiv 3q^2 + 4q^3$, $C \equiv 2q^3$, $D \equiv 3q^2 - 2q^3$ and q is the ratio of the thickness of the salt-depleted layer to the particle radius. In the limit of $\phi_D \to 0$, the volume fraction of the bulk domain is given by $\alpha = 1 - (1 + q)^3 \phi_D$. As ϕ_D increases, particle–particle contacts reduce the volume of the local domain, thereby implying that $\alpha'' \equiv d^2\alpha/d\phi_D^2$ is positive. The parameter, q, characterizes the strength of the salting-out interactions in our model.

For p_D, in eqn (3), we propose the following expression:

$$p_D = \left(1 + b\phi_D + \frac{e}{RT}\phi_D\right)\phi_D \tag{6}$$

where the first term in parenthesis represents the ideal contribution to osmotic pressure while $b(\phi_D)$ and $e(\phi_D)$ are temperature-independent functions describing the steric entropic term and the energetic contribution of dendrimer–dendrimer interactions, respectively. The expression of $b(\phi_D)$ is obtained from the Carnahan–Starling equation of state for hard spheres:[93]

$$b(\phi_D) = \frac{4 - 2\phi_D}{(1 - \phi_D)^3} \tag{7}$$

The quantity $e(\phi_D)$ can be linked to the excess internal energy of the dendrimer particles in the absence of the bulk domain. This will be described by introducing the intensive properties, $\omega_D \equiv U_D V_D/V$, where U_D is the excess internal energy and V the

total volume. The thermodynamic link between $\omega_D(\phi_D)$ and $e(\phi_D)$ is given by

$$\omega_D = \phi_D \tilde{e}(\phi_D) \tag{8}$$

where $\tilde{e}(\phi_D) \equiv \int_0^{\phi_D} e(x)dx$, with x being the integration variable and $\tilde{e}(0) = 0$ (see ESI† for details).

3.6 Excess internal energy

The excess internal energy associated with dendrimer–dendrimer interactions can be obtained from measurements of heat associated with the dilution of the dendrimer particles (see Fig. 5A). Specifically, we have measured the differential heat associated with consecutive injections of concentrated dendrimer solutions (titrant) into an initially dendrimer-free solution (titrand). We expect that electrostatic and pH effects associated with the dendrimer net charge and acid–base properties of the tertiary amines are negligible in our ternary mixtures but become important at very low ionic strengths. Thus, we have used a buffer aqueous solution with pH = 7.0 and an ionic strength of 0.14 instead of pure water as the titrand. As can be seen from the dilution power peaks and the corresponding values of differential heats in Fig. 5B and C, dendrimer dilution is an exothermic process. As dendrimer dilution occurs, dendrimer–dendrimer contacts correspondingly decrease thereby increasing the average exothermic hydration per dendrimer particle. This implies that dendrimer–dendrimer net interactions in water are endothermic.

The cumulative heat $V_D Q/V$ in eqn (2) is linked to ω_D by applying

$$\frac{V_D Q}{V} = \omega_D(\phi_D) - \frac{\phi_D}{\phi_D^0}\omega_D(\phi_D^0) \tag{9}$$

where ϕ_D^0 is the dendrimer volume fraction of the titrant solution, and $\phi_D \ll \phi_D^0$ is the dendrimer volume fraction inside the ITC cell after a given titrant injection. Note that a simple extrapolation of differential-heat values to $\phi_D \to 0$ gives estimates of $\omega_D(\phi_D^0)$. However, to extract accurate energy values, an analytical expression of ω_D in eqn (9) is needed. This can be obtained from the energy equation[86]

$$\omega_D = \frac{2\pi\phi_D^2}{V_D}\int_0^\infty r^2 u(r)g(r)dr \tag{10}$$

where $u(r)$ is the pairwise particle–particle potential energy, r is the particle–particle distance and $g(r)$ is the corresponding radial distribution function. Accurate radial distribution functions for interacting colloidal suspensions are available.[94] In our case, we examine the accuracy of two simple expressions of $g(r)$ associated with the two limiting cases of infinitely long and infinitely short range of interactions using the observed dependence of ω_D on ϕ_D. Using eqn (10), we have first examined the van der Waals[83] limiting expression of $\omega_D = \varepsilon\phi_D^2$, obtained by setting $g(r) \equiv 1$ in eqn (10), where ε is a constant energy parameter (positive for repulsive interactions). However, the experimental dependence of ω_D on ϕ_D was found to be appreciably stronger than that predicted by this simple quadratic expression. A more accurate representation of our ITC results is achieved by considering the range of dendrimer–dendrimer
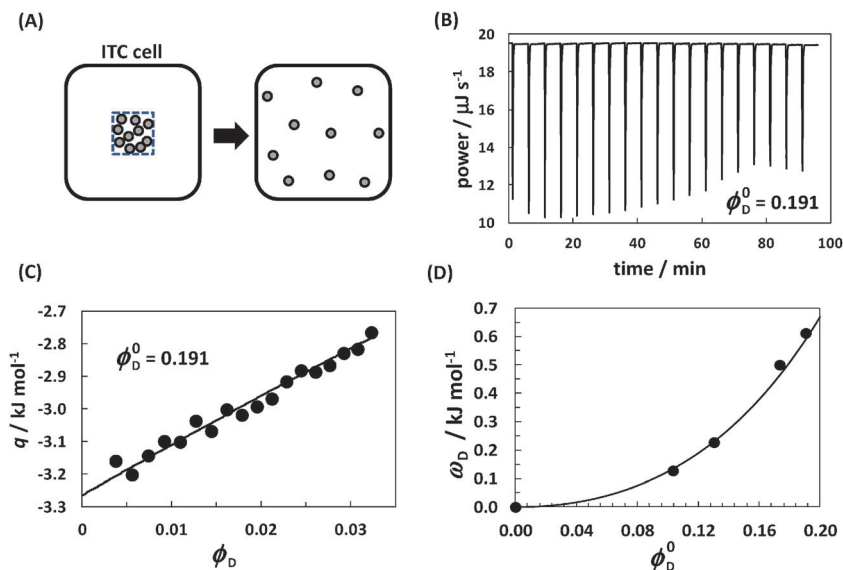
Fig. 5 (A) Scheme describing the dilution process from the dendrimer volume fraction, ϕ_D^0 (left) to ϕ_D (right) occurring inside the ITC cell. (B) Representative ITC power−time profile associated with consecutive injections of titrant solution ($\phi_D^0 = 0.191$) into the titrand solution inside the ITC cell. (C) Differential heat, q, extracted from the shown power−time profile as a function of dendrimer volume fraction inside the ITC cell, ϕ_D, after each injection. The solid curve is a fit through the data based on eqn (2), (9) and (11). (D) Reduced excess internal energy, ω_D, as a function of ϕ_D^0. The solid curve is a fit through the data based on eqn (11).

interactions as infinitely short. In other words, we assume that dendrimer dehydration occurs only when dendrimer particles are in close contact. To obtain the corresponding analytical expression of ω_D, we set $u(r) = \varepsilon V_D \delta(r - \sigma)$ with $r \geq \sigma$, where σ is the particle diameter, ε is the energy parameter and $\delta(r - \sigma)$ is the radial Dirac function with $4\pi \int_0^\infty r^2 \delta(r - \sigma) dr = 1$. For $g(r)$, eqn (10), we take the Carnahan–Starling contact value of $g(\sigma) = (1 - \phi_D/2)/(1 - \phi_D)^3$.[86] Thus eqn (10) becomes

$$\omega_D(\phi_D) = \frac{\varepsilon}{8} b(\phi_D) \phi_D^2 \qquad (11)$$

The expressions of $\omega_D(\phi_D)$ and $\omega_D(\phi_D^0)$ given by eqn (11) are first inserted into eqn (9). The resulting expression for $V_D Q/V$ is then inserted into eqn (2) so that a value of ε and $\omega_D(\phi_D^0)$ can be determined for a given ITC experiment. As we can see in Table 3, the values of ε are in good agreement with each other, thereby supporting the validity of eqn (11). A unique value of ε is obtained by applying the method of least squares based on eqn (11) to the $\omega_D(\phi_D^0)$ data in Fig. 5D. We obtain $\varepsilon = (19.9 \pm 0.3)$ kJ mol^{-1}, which corresponds to $\varepsilon/RT = 8.0 \pm 0.1$ at 25 °C.

3.7 Binodal curve

The experimental LLPS properties at 25 °C are described by an isothermal curve in the (C_S, ϕ_D) phase diagram known as the

binodal curve. We extract the experimental binodal at 25 °C by interpolating the turbidity data in Fig. 1B and D. The corresponding experimental data are shown in Fig. 6. We then construct a theoretical binodal starting from the equation of state discussed in Section 3.4. After inserting eqn (6) into eqn (3), we obtain

$$p = (1 + b\phi_D)\phi_D + \frac{1}{8}\frac{\varepsilon}{RT}(b + b'\phi_D)\phi_D^2 - (1 - \alpha + \phi_D\alpha')p_S \qquad (12)$$

with $e(\phi_D) = (\varepsilon/8)(b + b'\phi_D)\phi_D$ from eqn (8) and (11). The corresponding expression for $\mu \equiv (\mu_D - \mu_D^0)/RT$, where μ_D is the dendrimer chemical potential and μ_D^0 its standard value, is obtained
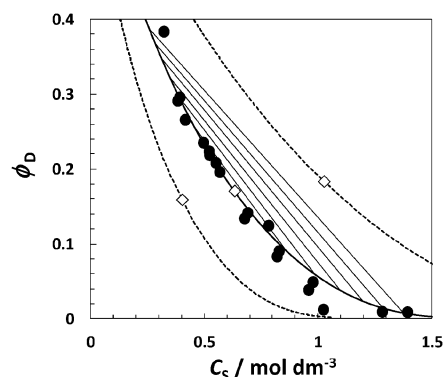

Fig. 6 Binodal data, ϕ_D as a function of C_S, for the dendrimer−salt−water system at 25 °C (solid circles). The solid curve is the theoretical binodal with $q = 0.35$. The solid lines are the corresponding calculated tie-lines. The dashed curves on the left and right sides are theoretical binodal with $q = 0.40$ and $q = 0.30$, respectively. The open diamonds represent the location of the critical point for each binodal curve.

Table 3 ITC parameters at 25 °C

ϕ_D	ε/kJ mol^{-1}	ω_D/kJ mol^{-1}
0.103	18.1	0.127
0.130	18.8	0.227
0.173	20.6	0.500
0.191	19.8	0.612

This journal is © the Owner Societies 2015

Phys. Chem. Chem. Phys., 2015, **17**, 28818–28829 | **28825**

from eqn (12) by applying the Gibbs–Duhem condition: $\phi_D(\partial\mu/\partial\phi_D)_{T,p_S} = (\partial p/\partial\phi_D)_{T,p_S}$:

$$\mu = \left(\ln\phi_D + \tilde{b} + b\phi_D\right) + \frac{1}{8}\frac{\varepsilon}{RT}(2b + b'\phi_D)\phi_D - \alpha'p_S \quad (13)$$

where $\tilde{b}(\phi_D) \equiv \int_0^{\phi_D} b(x)\mathrm{d}x$.

To construct the theoretical binodal, q in the expression of α is left as the only parameter to be varied. For a given value of q, the theoretical binodal is calculated in the following way. We start from a value of p_S that is just high enough to produce a non-monotonic behavior of $p(\phi_D)$ and $\mu(\phi_D)$. At this value of p_S, we numerically determine the values of $\phi_D^{(I)}$ and $\phi_D^{(II)}$ that satisfy the equilibrium conditions: $p(\phi_D^{(I)}) = p(\phi_D^{(II)})$ and $\mu(\phi_D^{(I)}) = \mu(\phi_D^{(II)})$. This procedure is then repeated for higher values of p_S. The corresponding salt concentrations are obtained by first extracting C_S^* from eqn (4) and then applying $C_S^{(I)} = C_S^*\alpha(\phi_D^{(I)})$ and $C_S^{(II)} = C_S^*\alpha(\phi_D^{(II)})$. The compositions of the two coexisting phases, $(C_S^{(I)},\phi_D^{(I)})$ and $(C_S^{(II)},\phi_D^{(II)})$, are connected by tie lines (solid lines in Fig. 6). The critical point is calculated by the linear extrapolation of $(\phi_D^{(I)} + \phi_D^{(II)})/2$ and p_S to $|\phi_D^{(II)} - \phi_D^{(I)}|^{1/\beta} \to 0$, where $\beta = 0.5$ is the appropriate exponent for this model.

As q increases, the theoretical binodal curve horizontally shifts towards lower salt concentrations, together with the critical salt concentration, $C_S^{(c)}$. This reflects the increasing strength of the salting-out agent. As shown in Fig. 6, the theoretical binodal is in good agreement with the experimental data when $q = 0.35$. Correspondingly, we obtain $C_S^{(c)} = 0.63$ mol dm^{-3} and $\phi_D^{(c)} = 0.17$, in good agreement with our experimental findings (see Section 3.2). The proposed model also predicts the experimental slope, $(\partial C_S/\partial\phi_D)_T$, at the critical point. We obtain: $(\partial C_S/\partial\phi_D)_T = -(2.4 \pm 0.1)$ mol dm^{-3} by fitting our experimental data in Fig. 6 around the critical point (see ESI† for details), which is in excellent agreement with the value of -2.37 mol dm^{-3} calculated from the model with $q = 0.35$. Thus, the proposed one-parameter model can predict two features of the binodal that are thermodynamically independent of each other: the location of the critical point and the boundary slope around the critical point. However, some deviation between the experimental and the model appears at salt concentrations around ≈ 1 mol dm^{-3}.

The slope, $(\partial C_S/\partial\phi_D)_T$, at the critical point also represents the limiting value of the salt–dendrimer partitioning coefficient, $\Delta C_S/\Delta\phi_D$, at this point as discussed in Section 3.2. It is important to note that the value obtained from the turbidity data is in agreement with that obtained from partitioning data within the experimental error. Furthermore, these salt–dendrimer partitioning data can also be used to extract values of q by applying the condition

$$C_S^* = \frac{C_S^{(I)}}{\alpha\left(\phi_D^{(I)}\right)} = \frac{C_S^{(II)}}{\alpha\left(\phi_D^{(II)}\right)} \quad (14)$$

The calculated q values, which are also included in Table 1, are comparable with $q = 0.35$ and range from 0.25 to 0.34. These variations can be attributed to the large experimental error associated with the partitioning coefficients in Table 1.

Finally, we have also used our thermodynamic model to examine the behavior of the DLS diffusion coefficient. In the limit of $\phi_D \to 0$, D_{DLS} can be written as

$$D_{DLS} = D_0[1 + (k_H + k_S)\phi_D] \quad (15)$$

where k_H and k_S are two parameters describing hydrodynamic and thermodynamic interactions, respectively.[83,84] Since $(\partial p/\partial\phi_D)_{T,p_S} = 1 + k_S\phi_D$ in the limit of $\phi_D \to 0$, eqn (12) yields

$$k_S = 8 + \frac{\varepsilon}{k_B T} - \alpha''(0)p_S \quad (16)$$

with $\alpha''(0) = (12 + 15q + 6q^2 + q^3)q^3$. If we assume that the hydrodynamic parameter, k_H, is independent of salt concentration and temperature, and set the value of k_D at $C_S = 0.05$ mol dm^{-3} and 25 °C as the reference, the agreement of the other values of k_D in Table 2 with theoretical predictions is achieved when $q = 0.33$. When, instead, we set $q = 0.35$, the predicted value of k_D at $C_S = 0.95$ mol dm^{-3} is about 20% lower than that reported in Table 2. This is still an acceptable result considering that we have approximated k_H as a constant. Our model also predicts that the temperature dependence of k_D is small, consistent with our findings (see ESI† for details).

3.8 LLPS thermal behavior

We now examine the anomalous temperature response discussed in Section 3.1. The observed thermal behavior can be thought as the net result of at least two thermodynamic factors of comparable contribution but with opposite temperature responses. Thus, a quantitative prediction of the behavior of $T_{ph}(C_S, \phi_D)$ is difficult to achieve. However, our model can be used to understand the two main features of LLPS: (1) LLPS switches from being induced by cooling to being induced by heating as C_S increases and ϕ_D correspondingly decreases (see Fig. 1(A–D)); and (2) the existence of a narrow composition domain in which LLPS can be induced by both increasing and decreasing temperature (see Fig. 2).

According to eqn (3), p_D, p_S and α are the three quantities regulating the thermodynamic behavior of the ternary dendrimer–salt–water system. The first quantity, p_D, describes the net dendrimer–dendrimer interactions in the absence of the bulk domain. Since our ITC results show that dendrimer–dendrimer interactions are endothermic, dendrimer–dendrimer repulsion decreases as temperature increases. The second quantity, p_S, describes salt thermodynamic non-ideality. According to osmotic-coefficient data,[90] p_S increases with temperature at any given salt concentration. Thus, the salt effectiveness in inducing LLPS increases with temperature. Clearly, the thermal behavior of both p_D and p_S indicates that LLPS should be induced only by heating. While this analysis is in agreement with the experimental behavior observed at low ϕ_D, it fails to predict the thermal behavior observed at high ϕ_D. To address this aspect within the framework of our model, we assume that the parameter q in the expression of α increases as temperature decreases. This implies that the salting-out strength of salt increases as temperature decreases.

As a numerical example, we compute the binodal at three representative temperatures, 25, 15 and 5 °C. The corresponding
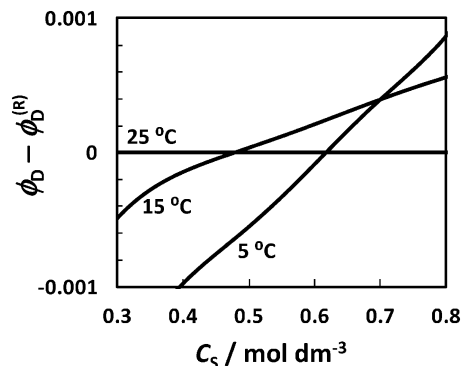
28826 | *Phys. Chem. Chem. Phys.*, 2015, **17**, 28818–28829

This journal is © the Owner Societies 2015

Paper

Fig. 7 Calculated relative binodal curves, $\phi_D - \phi_D^{(R)}$, as a function of C_S, where $\phi_D^{(R)}$ represents the binodal at 25 °C. The numbers associated with each curve identify the corresponding value of temperature. The values of q for the binodal curves at 25, 15 and 5 °C are 0.3500, 0.3544 and 0.3604, respectively.

values of $q(T)$ are chosen to be 0.3500, 0.3544 and 0.3604, respectively. In Fig. 7, we plot $\phi_D - \phi_D^{(R)}$ as a function of C_S, where $\phi_D^{(R)}(C_S)$ represents the binodal curve at 25 °C set as the reference. The three relative boundaries are shown in this figure with that at 25 °C being located at $\phi_D - \phi_D^{(R)} \equiv 0$. Points below and above a given boundary correspond to homogenous mixtures and biphasic systems at the boundary temperature, respectively. According to the computed curves, a point on the 15 °C binodal at $C_S \approx 0.3$ mol dm^{-3} represents a homogeneous mixture at 25 °C but a biphasic system at 5 °C. On the other hand, a point on the same binodal at $C_S \approx 0.8$ mol dm^{-3} is associated with the opposite thermal behavior. This is in agreement with our experiment results in Fig. 1A–D. Moreover, note that the binodal at 15 °C is located above the other two binodals when $C_S \approx 0.5$–0.6 mol dm^{-3}. Thus, at these intermediate salt concentrations, a point slightly below the 15 °C binodal represents a homogeneous mixture at 15 °C but a biphasic system at both 5 °C and 25 °C. This is in agreement with the thermal behavior illustrated in Fig. 2.

The proposed model successfully predicts that cooling-induced LLPS occurs at high ϕ_D. This can be understood by recognizing that an increase in p_S favors LLPS. Thus, we examine the dependence of p_S on temperature at constant C_S based on the observation that p_S is directly proportional to $\varphi C_S^\star$ (see eqn (4)) with $C_S^\star = C_S/\alpha$. If α is independent of temperature, p_S increases with T due to the corresponding increase in the salt osmotic coefficient, φ. Under these conditions, LLPS can only be favored by heating. However, if α is a function of temperature, then the corresponding temperature dependence of $C_S^\star$ (at constant C_S) will also contribute to the behavior of p_S. In our numerical example, α increases with T, thereby implying that p_S may decrease as T increases if the temperature dependence of α is sufficiently strong. Under these conditions, LLPS will be favored by cooling. It is important to remark that this effect is expected to prevail at relatively high ϕ_D. Indeed, according to the proposed model, LLPS is expected to be always favored by heating at sufficiently low ϕ_D since α becomes independent of temperature in the limit of $\phi_D \to 0$; *i.e.*, $\alpha \to 1$ independent of $q(T)$.

4. Conclusions

LLPS of aqueous solutions of the PAMAM G4–OH dendrimer in the presence of sodium sulfate was observed. To explain the experimental binodal at 25 °C, a thermodynamic model, which includes dendrimer–dendrimer interaction energy (ε), salting-out strength of salt (q) and the available salt osmotic coefficient (φ) of the binary salt–water system, was developed. Parameter ε was characterized by ITC so that q remains the only parameter to be determined. It was shown that the model agrees with both the location of the experimental binodal and its slope around the critical point when $q = 0.35$. The proposed thermodynamic model also predicts that the observed unusual temperature behavior can be explained if $\varphi(T)$ and $q(T)$ have opposite temperature effects on LLPS, with $\varphi(T)$ dominating at low ϕ_D and $q(T)$ prevailing at high ϕ_D. This work contributes to the fundamental understanding of the phase behavior of dendrimer aqueous solutions and the effect of salting-out agents on macromolecules in general. Our experimental findings and theoretical model apply to the PAMAM–OH dendrimer chosen in this investigation. Nevertheless, these studies can be used as the starting reference point for LLPS studies on other dendrimer systems. One important aspect to investigate will be how the LLPS behavior depends on the composition of surface terminal groups.

This investigation also provides guidance for the development of LLPS-based methods for guest encapsulation and the preparation of novel dendrimer materials. For example, guest molecules could be first added to a dendrimer aqueous solution at very low ionic strengths. Under these conditions, guest encapsulation is favored by the more open conformational state assumed by dendrimers. In a second step, non-toxic salts such as sodium sulfate could be added to the solution in order to promote a more compact conformational state of the guest-loaded dendrimers and induce dendrimer condensation (LLPS). This would result in the separation of the loaded dendrimer-rich phase from the remaining aqueous solution. As a second potential application, the coacervation of low-generation dendrimers could be exploited to produce dendrimer nano/microspheres with high guest loading capacity. This would circumvent the need of preparing high-generation dendrimers, which are relatively hard to synthesize, poorly soluble and sterically hindered.

Acknowledgements

References

1 J. Seuring and S. Agarwal, *ACS Macro Lett.*, 2013, **2**, 597–600.
2 A. A. Hyman and K. Simons, *Science*, 2012, **337**, 1047–1049.
3 P. Li, S. Banjade, H. C. Cheng, S. Kim and B. Chen, *et al.*, *Nature*, 2012, **483**, 336–340.
4 C. D. Keating, *Acc. Chem. Res.*, 2012, **45**, 2114–2124.
5 Y. Wang, A. Lomakin, R. F. Latypov and G. B. Benedek, *Proc. Natl. Acad. Sci. U. S. A.*, 2011, **108**, 16606–16611.

This journal is © the Owner Societies 2015

Phys. Chem. Chem. Phys., 2015, **17**, 28818–28829 | 28827

6 A. Stradner, H. Sedgwick, F. Cardinaux, W. C. K. Poon, S. U. Egelhaaf and P. Schurtenberger, *Nature*, 2004, **432**, 492–495.

7 Y. Zhang and P. S. Cremer, *Proc. Natl. Acad. Sci. U. S. A.*, 2009, **106**, 15249–15253.

8 Y. Zhang and P. S. Cremer, *Annu. Rev. Phys. Chem.*, 2010, **61**, 63–83.

9 D. L. Elbert, *Acta Biomater.*, 2011, **7**, 31–56.

10 A. C. Lima, P. Sher and J. F. Mano, *Expert Opin. Drug Delivery*, 2012, **9**, 231–248.

11 Y. Wang and O. Annunziata, *Langmuir*, 2008, **24**, 2799–2807.

12 M. D. Nichols, E. A. Scott and D. L. Elbert, *Biomaterials*, 2009, **30**, 5283–5291.

13 H. D. Willauer, J. G. Huddleston and R. D. Rogers, *Ind. Eng. Chem. Res.*, 2002, **41**, 1892–1904.

14 P. A. Albertsson, *Partition of Cell Particles and Macromolecules*, Wiley, New York, 1986.

15 A. Behr, G. Henze and R. Schomäcker, *Adv. Synth. Catal.*, 2006, **348**, 1485–1495.

16 F. Joo, *Acc. Chem. Res.*, 2002, **35**, 738–745.

17 M. L. Broide, C. R. Berland, J. Pande, O. Ogun and G. B. Benedek, *Proc. Natl. Acad. Sci. U. S. A.*, 1991, **88**, 5660–5664.

18 O. Galkin, K. Chen, R. L. Nagel, R. E. Hirsch and P. G. Vekilov, *Proc. Natl. Acad. Sci. U. S. A.*, 2002, **99**, 8479–8483.

19 P. R. Ten Wolde and D. Frenkel, *Science*, 1997, **277**, 1975–1978.

20 O. Galkin and P. G. Vekilov, *Proc. Natl. Acad. Sci. U. S. A.*, 2000, **97**, 6277–6281.

21 D. A. Tomalia, A. M. Naylor and W. A. Goddard, *Angew. Chem., Int. Ed.*, 1990, **29**, 138–175.

22 U. Boas, J. B. Christensen and P. M. H. Heegaard, *J. Mater. Chem.*, 2006, **16**, 3785–3798.

23 J. F. G. A. Jansen, E. M. M. de Brabander-van den Berg and E. W. Meijer, *Science*, 1994, **18**, 1226–1229.

24 J. Lim, G. M. Pavan, O. Annunziata and E. Simanek, *J. Am. Chem. Soc.*, 2012, **134**, 1942–1945.

25 R. M. Crooks, M. Zhao, L. Sun, V. Chechik and L. K. Yeung, *Acc. Chem. Res.*, 2001, **34**, 181–190.

26 S. H. Medina and M. E. H. El-Sayed, *Chem. Rev.*, 2009, **109**, 3141–3157.

27 A. E. Beezer, A. S. H. King, I. K. Martin, J. C. Mitchell, L. J. Twyman and C. F. Wain, *Tetrahedron*, 2003, **59**, 3873–3880.

28 B. K. Nanjwade, H. M. Bechra, G. K. Derkar, F. V. Manvi and V. K. Nanjwade, *Eur. J. Pharm. Sci.*, 2009, **38**, 185–196.

29 A.-M. Caminade, A. Ouali, M. Keller and J.-P. Majoral, *Chem. Soc. Rev.*, 2012, **41**, 4113–4125.

30 S. K. Oh, Y. H. Niu and R. M. Crooks, *Langmuir*, 2005, **21**, 10209–10213.

31 M. S. Diallo, S. Christie, P. Swaminathan, J. H. Johnson and W. Goddard, *Environ. Sci. Technol.*, 2005, **39**, 1366–1377.

32 L. M. Bronstein and Z. B. Shifrina, *Chem. Rev.*, 2011, **111**, 5301–5344.

33 A. P. H. J. Schenning, C. Elissen-Roman, J. W. Weener, M. W. P. L. Baars, S. J. van der Gaast and E. W. Meijer, *J. Am. Chem. Soc.*, 1998, **120**, 8199–8208.

34 H. G. Lang, S. Maldonado, K. J. Stevenson and B. D. Chandler, *J. Am. Chem. Soc.*, 2004, **126**, 12949–12956.

35 J. M. J. Fréchet, *Proc. Natl. Acad. Sci. U. S. A.*, 2002, **99**, 4782–4787.

36 D. Astruc, E. Boisselier and C. Ornelas, *Chem. Rev.*, 2010, **110**, 1857–1959.

37 Y. Haba, A. Harada, T. Takagishi and K. Kono, *J. Am. Chem. Soc.*, 2004, **126**, 12760–12761.

38 C. Kojima, K. Yoshimura, A. Harada, Y. Sakanishi and K. Kono, *J. Polym. Sci., Part A: Polym. Chem.*, 2010, **48**, 4047–4054.

39 W. Li, A. Zhang, Y. Chen, K. Feldman, H. Wu and A. D. Schlüter, *Chem. Commun.*, 2008, 5948–5950.

40 Y. Shen, X. Ma, B. Zhang, Z. Zhou, Q. Sun and E. Jin, *et al.*, *Chem. – Eur. J.*, 2011, **17**, 5319–5326.

41 T. Koga, M. Iimura and N. Higashi, *Macromol. Biosci.*, 2012, **12**, 1043–1047.

42 M. C. Parrott, J. F. Valliant and A. Adronov, *Langmuir*, 2006, **22**, 5251–5255.

43 Z. Jia, H. Chen, X. Zhu and D. Yan, *J. Am. Chem. Soc.*, 2006, **128**, 8144–8145.

44 J. G. Jang, S. Noh and Y. C. Bae, *J. Phys. Chem. A*, 2000, **104**, 7404–7407.

45 A. N. Rissanou, I. G. Economou and A. Z. Panagiotopoulos, *Macromolecules*, 2006, **39**, 6298–6305.

46 L. Lue and J. M. Prausnitz, *Macromolecules*, 1997, **30**, 6650–6657.

47 L. M. Kaminskas, V. M. McLeod, C. J. H. Porter and B. J. Boyd, *Mol. Pharmaceutics*, 2012, **9**, 355–373.

48 A. Buczkowski, S. Sekowski, A. Grala, D. Palecz and K. Milowska, *et al.*, *Int. J. Pharm.*, 2011, **408**, 266–270.

49 D. Astruc, *Nat. Chem.*, 2012, **4**, 255–267.

50 M. Zhao, L. Sun and R. M. Crooks, *J. Am. Chem. Soc.*, 1998, **120**, 4877–4878.

51 P. K. Maiti, C. Tahir, G. Wang and W. A. Goddard, *Macro-molecules*, 2004, **37**, 6236–6254.

52 Y. Liu, V. S. Bryantsev, M. S. Diallo and W. Goddard, *J. Am. Chem. Soc.*, 2009, **131**, 2798–2799.

53 P. K. Maiti, Y. Li, T. Cagin and W. Goddard, *J. Chem. Phys.*, 2009, **130**, 144902.

54 P. K. Maiti, T. Çağın, S.-T. Lin and W. Goddard, *Macro-molecules*, 2005, **38**, 979–991.

55 M. Ballauff and C. N. Likos, *Angew. Chem., Int. Ed.*, 2004, **43**, 2998–3020.

56 A. Mecke, I. Lee, J. R. Baker, M. M. B. Holl and B. G. Orr, *Eur. Phys. J. E: Soft Matter Biol. Phys.*, 2004, **14**, 7–16.

57 I. Lee, B. D. Athey, A. W. Wetzel, W. Meixner and J. R. Baker, *Macromolecules*, 2002, **35**, 4510–4520.

58 L. Porcar, K. Hong, P. D. Butler, K. W. Herwig, G. S. Smith, Y. Liu and W.-R. Chen, *J. Phys. Chem. B*, 2010, **114**, 1751–1756.

59 L. Porcar, Y. Liu, R. Verduzco, K. Hong, P. D. Butler, L. J. Magid, G. S. Smith and W.-R. Chen, *J. Phys. Chem. B*, 2008, **112**, 14772–14778.

60 S. Rathgeber, T. Pakula and V. Urban, *J. Chem. Phys.*, 2004, **121**, 3840–3853.

61 W. Chen, L. Porcar, Y. Liu, P. D. Butler and L. J. Magid, *Macromolecules*, 2007, **40**, 5887–5898.

62 S. Stechemesser and W. Eimer, *Macromolecules*, 1997, **30**, 2204–2206.

63 W. Tian and Y. Ma, *Soft Matter*, 2010, **6**, 1308–1316.

64 A. Topp, B. J. Bauer, D. A. Tomalia and E. J. Amis, *Macromolecules*, 1999, **32**, 7232–7237.

65 P. K. Maiti and B. Bagchi, *J. Chem. Phys.*, 2009, **131**, 214901.

66 P. Welch and M. Muthukumar, *Macromolecules*, 1998, **31**, 5892–5897.

67 K. P. Ananthapadmanabhan and E. D. Goddard, *Langmuir*, 1987, **3**, 25–31.

68 J. A. Rard and D. G. Miller, *J. Solution Chem.*, 1979, **8**, 755–766.

69 A. Nourse, D. B. Millar and A. P. Minton, *Biopolymers*, 2000, **53**, 316–328.

70 Y. Wang and O. Annunziata, *J. Phys. Chem. B*, 2007, **111**, 1222–1230.

71 V. C. P. da Costa, B. J. Hwang, S. E. Eggen, M. J. Wallace and O. Annunziata, *J. Chem. Thermodyn.*, 2014, **75**, 119–127.

72 Y. Wang and O. Annunziata, *Langmuir*, 2008, **24**, 2799–2807.

73 A. Lomakin, D. B. Teplow and G. B. Benedek, *Methods Mol. Biol.*, 2005, **299**, 153–174.

74 Y. Niu, L. Sun and R. M. Crooks, *Macromolecules*, 2003, **36**, 5725–5731.

75 A. C. Dumetz, A. M. Snellinger-O'Brien, E. W. Kaler and A. M. Lenhoff, *Protein Sci.*, 2007, **16**, 1867–1877.

76 S. N. Timasheff, *Proc. Natl. Acad. Sci. U. S. A.*, 2002, **99**, 9721–9726.

77 M. T. Record and C. F. Anderson, *Biophys. J.*, 1995, **68**, 786–794.

78 V. A. Parsegian, R. P. Rand and D. C. Rau, *Proc. Natl. Acad. Sci. U. S. A.*, 2000, **97**, 3987–3992.

79 M. S. McAfee, H. Zhang and O. Annunziata, *Langmuir*, 2014, **30**, 12210–12219.

80 C. Tan, J. G. Albright and O. Annunziata, *J. Phys. Chem. B*, 2008, **112**, 4967–4974.

81 O. Annunziata, D. Buzatu and J. G. Albright, *Langmuir*, 2005, **21**, 12085–12089.

82 A. Korosi and B. M. Fabuss, *J. Chem. Eng. Data*, 1968, **13**, 548–552.

83 M. Muschol and F. Rosenberger, *J. Chem. Phys.*, 1995, **103**, 10424–10432.

84 B. M. Fine, A. Lomakin, O. O. Ogun and G. B. Benedek, *J. Chem. Phys.*, 1996, **104**, 326–335.

85 D. L. Richter-Egger, J. C. Landry, A. Tesfai and S. A. Tucker, *J. Phys. Chem. A*, 2001, **105**, 6826–6833.

86 J.-P. Hansen and I. R. McDonald, *Theory of simple liquids*, 4th edn, Academic Press, Oxford, 2013.

87 A. Lomakin, N. Asherie and G. B. Benedek, *J. Chem. Phys.*, 1996, **104**, 1646–1656.

88 H. N. W. Lekkerkerker, W. C. K. Poon, P. N. Pusey, A. Stroobants and P. B. Warren, *Europhys. Lett.*, 1992, **20**, 559–564.

89 S. M. Ilett, A. Orrock, W. C. K. Poon and P. N. Pusey, *Phys. Rev. E: Stat. Phys., Plasmas, Fluids, Relat. Interdisc. Top.*, 1995, **51**, 1344–1352.

90 J. A. Rard, S. L. Clegg and D. A. Palmer, *J. Solution Chem.*, 2000, **29**, 1–49.

91 G. A. Mansoori, N. F. Carnahan, K. E. Starling and T. W. Leland Jr., *J. Chem. Phys.*, 1971, **54**, 1523–1525.

92 S. Amokrane and C. Regnaut, *Phys. Rev. E: Stat. Phys., Plasmas, Fluids, Relat. Interdisc. Top.*, 1996, **53**, 1990–1993.

93 N. F. Carnahan and K. E. Starling, *J. Chem. Phys.*, 1969, **51**, 635–636.

94 C. Caccamo, G. Pellicane, D. Costa, D. Pini and G. Stell, *Phys. Rev. E: Stat. Phys., Plasmas, Fluids, Relat. Interdiscip. Top.*, 1999, **60**, 5533–5543.

This journal is © the Owner Societies 2015

Phys. Chem. Chem. Phys., 2015, **17**, 28818–28829 | 28829